Proceedings of the 3rd Annual
IEEE Conference on Automation Science and Engineering
Scottsdale, AZ, USA, Sept 22-25, 2007

Characterization of Program Controlled CO_2 Laser-Cut PDMS Channels for Lab-on-a-chip Applications

Andrew W. Holle, Shih-Hui Chao, Mark R. Holl, *IEEE Member*,
Jeffrey M. Houkal, and Deirdre R. Meldrum, *IEEE Fellow*

***Abstract*—PDMS (polydimethylsiloxane) is an important material for lab-on-a-chip, an emerging technology to automate biological and chemical operations in microfluidic devices. Laser manufacturing of materials suitable for use in laminate-based construction of lab-on-a-chip devices is an important step in the development of automated assembly line procedures. This study investigates the effect of laser cutting parameters on channel topography when a carbon dioxide laser is used to create trenches in PDMS. We present cross-sectional micrographs of the laser-ablated channels that reveal a modified Gaussian contour, with smooth, circular arcs at the bottom of the channel. We define geometric parameters that describe the contours, including cut depth and maximum cut width. Relationships between laser power, pulses per inch, and laser traverse speed and ablation profile patterns are established. A strong linear relationship (R^2=0.9951) between cut depth and laser power is demonstrated. Analysis of the radii of circular arcs at the bottom of the channel and at the surface of the PDMS was performed. As laser power density is increased (increase in laser power or pulses per inch) the PDMS surface radii and channel floor radius decrease.**

I. Introduction

Lab-on-a-chip is a rapidly emerging field in which small (micro and nanoliter scale) volumes of fluids are manipulated for the sake of an experiment. In order to manipulate fluids on this scale, channels with appropriate dimensions (typically 10 to 100 micrometers) are needed. The silicon-based organic polymer PDMS has been used extensively in lab-on-a-chip applications. Small features in PDMS are commonly achieved photolithographically, but this is time consuming and costly.

Laser cutting has been used as an alternative to photolithography. Past works have focused on the engraving of PDMS with lasers, but the majority of them utilize expensive Ti:sapphire femtosecond laser systems [1]. Wolfe et al. used a femtosecond laser to etch channels in PDMS and to produce intricate 2D patterns for lab-on-a-chip applications [2], but this research did not characterize channel geometry. Kim, Campbell, Groisman, Kleinfeld and Schaffer also utilized a femtosecond laser to build unmoldable features into microfluidc devices [3]. This work addressed soft lithography's inability to realize 3D structures. Femtosecond lasers were utilized in Nguyen et al.'s research on bioreactors [4]. Seven polymer layers, four of them PDMS, were machined with femtosecond lasers, then stacked and bonded to form a complex bioreactor. This work proposed a five-minute ultrasonic cleaning to remove debris from the PDMS. While both of these works address certain challenges with the laser machining of PDMS, neither attempts to increase understanding of the channel dimensions and topography that laser cutting provides.

Other works have addressed channel characteristics of laser-machined polymers. Chan, Nguyen, Xia, and Wu used a CO_2 laser similar to the one used in this investigation to micromachine channels in PMMA (Polymethylmethacrylate) for use in fuel cells [5]. These channels exhibited a distinctive Gaussian profile. Channel cross sections were shown but not quantitatively characterized or modeled.

Still other works have set out to understand selected characteristics of the surfaces of laser machined polymers. Pugmire, Waddell, Haasch, Tarlov, and Locascio analyzed the surface chemistry and electroosmotic flow characteristics of channels cut into several polymers [6], including PMMA, PETG (polyethylene terephthalate glycol), PC (polycarbonate), and PVC (polyvinyl chloride). PDMS was not characterized. Pham et al. correlated laser ablation rate with the thermal properties of several polymers, including PDMS [7].

Graubner et al. quantified the relationship between pulse number and feature depth for isolated laser-ablated holes in PDMS [8]. An Nd:YAG laser was used to machine single holes into PDMS. Using this design, plots of depth vs. number of pulses were generated. Hole profiles and lateral dimensions were not analyzed.

The CO_2 laser is a cost-effective option for fabricating PDMS channels with widths larger than 100 micrometers. We characterized the topography of laser-cut channels at various laser settings. Data of the type presented here may be helpful in laser parameter selection for creating channels in PDMS sheets.

Manuscript received March 18, 2007. This work was supported in part by the National Institutes of Health NHGRI Centers of Excellence in Genomic Science (Grant 5 P50 HG002360, D. Meldrum (PI)).

A.W. Holle is with the Harrington Department of Bioengineering, Arizona State University, Tempe, AZ 85287-9309 USA. (e-mail: Andrew.Holle@asu.edu; phone: 860-861-1303)

D.R. Meldrum is Director of the Center for Ecogenomics and the Dean of the Ira A. Fulton School of Engineering, Arizona State University, Tempe, AZ 85287-9309 USA (e-mail: Deirdre.meldrum@asu.edu)

S.H. Chao, J.M. Houkal, and M.R. Holl are with the Center for Ecogenomics, The Biodesign Institute, Arizona State University, Tempe, AZ 85287-6501 USA (e-mail: joe.chao@asu.edu; jeff.houkal@asu.edu; mark.holl@asu.edu).

II. Methods and Materials

A. PDMS

The PDMS used for this investigation was purchased from Specialty Silicone Products, Inc. (Ballston Spa, NY). The material was packaged in 300 millimeter by 300 millimeter sheet form and had a nominal thickness of 381 micrometers (0.015 inches), the thickest sheet available. Pre-made sheets were chosen to avoid potential inconsistencies.

B. Laser

The CO_2 laser used for this investigation was the XL-9200, manufactured by Universal Laser Systems Inc. (Scottsdale, AZ). Having a characteristic wavelength of 10.6 micrometers, the infrared laser operates with variable settings for power, speed, and pulses per inch (PPI). The assist gas utilized by this specific laser was air, supplied coaxially. Powers presented are relative to the maximum allowable input power of 60 watts (e.g. 50% power is equivalent to 30 watts). Speeds are fractions of the maximum speed of 254 cm/sec (e.g. 50% speed is equivalent to 127 cm/sec).

C. Channel Creation

To characterize the effect of laser parameters on channel morphology, a full spectrum of data was collected employing different laser settings. Two repetition rates (500 and 750 PPI) were used. Lower settings tended to produce a noticeable scalloping effect due to the larger distance between laser pulses. Four speed settings (25%, 50%, 75%, and 100%) were used to investigate the effect of laser speed on channel depth and shape. Ten power settings (10-100% in increments of 10%) were used to elucidate the effect of laser power and channel depth and shape. Eighty cuts were required in order to test each combination of these configurations. To do this, an AutoCad template with eighty contiguous parallel lines with length of 4.66 millimeters and spacing of 1.27 millimeters was prepared. A strip of PDMS was cut from the packaged sheet and positioned within the cutting field of the laser system in such a way that the pattern of parallel channel lines overlapped the edge of the strip. This was done to ensure that a clean cross-sectional profile was obtained at the edge of the strip, as opposed to cutting the PDMS cross section with a razor or scissors after the laser lines had been cut. The design was plotted on the XL-9200 seven lines at a time, due to the ability of the plotter to accommodate seven different laser settings in one pass. The assist gas was supplied in each experiment; no cuts were made without it in order to maintain the cleanliness of the lens. Once all eighty cuts had been made, the PDMS strip was washed with soap and water to remove debris. The strip was left to dry overnight between two composite wipes in a semi-clean room. After drying, the strip was cut into eight segments with ten lines each to facilitate imaging. After cross section characterization one 500 PPI and one 750 PPI channel were sectioned longitudinally to document the degree of scalloping within the trench.

D. Image Acquisition

Each of the eight strip segments was attached to a steel V-block using the natural adherence of the PDMS. The V-block served to position the samples in the field of view and to provide contrast between the PDMS and the background. Images were acquired at a magnification of 11.25x, with the exception of the scalloping test image. An example of the cross-sectional profile of cut PDMS is seen in Fig. 1. For reference, all figures shown have thicknesses of 381 micrometers.

E. Image Analysis

Photomicrographs were imported into MATLAB, where an image analysis function was used to calculate the parameters shown in Fig. 2. Measurements were taken for three radii, two slope values, and the depth and maximum width of the cut. The width was measured from the tangent intersections of the upper radii and the surface. Depth was measured from the bottom of the channel to the surface. To calculate the radii for the three circles, a circle-fit function was given a series of points anticipated to be on both the cut profile and the circle. This function then returned the center point and radius of the circle prescribed by the input points. Measurements were converted from pixels to metric units by calibration with a Standard USAF 1951 Resolution Test Pattern at the same magnification.

III. RESULTS

A. Scalloping Test

Fig. 3 is an orthogonal cross section of PDMS which shows the surface profile of the base of the channel. From this profile, it can be seen that scalloping has been kept to a minimum at the 500 PPI setting and thus at higher settings.

Results on the low end of the power spectrum, especially at high speeds, often would result in no cut. Because of this, there are several unattainable data points on the following graphs. An example of this is seen on all graphs at a speed setting of 100%.

B. Radius 1, 2, and 3

No strict patterns were found among the three radius parameters. However, gradual trends were noticed.

In several instances, especially when levels for power setting and speed setting were moderate (between 50% and 70% for power setting and between 25% and 50% for speed setting) all three transition regions were sloped, yielding a Gaussian cut profile. In these cases, the transition regions could be modeled well with arc segments of finite radius. Furthermore, the cut profile was moderately symmetrical, with both radii 1 and 3 being approximately equal. An example of this cut profile can be seen in Fig. 4.

In other cases, mainly in cases with both high speed setting and low power setting, all three transition regions

were sloped, but the overall profile was asymmetric. In a majority of these instances, radius 3 was greater than radius 1. An example of this is seen in Fig. 5. These cut profiles were mostly seen at high speed setting and low power setting configurations.

Another cut profile observed had one upper transition region sloped and the other blunt. In most cases, similar to the previous example, the region corresponding to radius 1 was the region undergoing the blunt transition, while the region corresponding to radius 3 kept its rounded, smooth transition profile. An example of this cut profile can be seen in Fig. 6. These cut profiles were mostly seen at high speed setting and high power setting levels.

The final group of cut profiles noticed was those in which both cut intersections were sharp. This 'cornering' yielded comparatively small radius values (under 25 micrometers) when the circle fit function in MATLAB was used. An example of this is seen in Fig. 7. These cut profiles were seen mostly at high power setting and low speed setting laser configurations.

Similarly, there was a great deal of variability in the data for radius 2. Overall, as power setting increased, the value for radius 2 decreased.

C. Width and Depth

Data for the channel depth and channel width were collected at both 500 and 750 PPI. The data collected for channel width is displayed in Fig. 8 and Fig. 9. There is a strong positive relationship between width and power setting, with linear regression R^2 values as high as 0.91. Furthermore, there is a clear trend that as speed setting is increased, channel width decreases, as expected. The data for channel depth is displayed in Fig. 10 and Fig. 11. There is a very strong positive relationship between depth and power setting. The linear regression at 50 percent speed at 500 PPI yielded an R^2 value of 0.995. All other R^2 values were relatively high.

D. Slope 1 and Slope 2

Slope 1 is the slope of the line on the left hand side of the cut, and therefore by definition must always be negative. Charts of slope 1 vs. power setting for four different speed settings are seen in Figs. 12 and 13. A somewhat strong inverse relationship is observed; as power setting increases, slope 1 gets more negative. Slope 2 is the slope of the right hand side of the cut, and must be positive by definition. Charts of slope 2 vs. power setting for four different speed settings are seen in Figures 14 and 15. A positive relationship is observed, with slope 2 increasing as power setting increases. There is a very strong positive relationship between slope and power setting. The linear regression at 50 percent speed at 500 PPI yielded an R^2 value of 0.995, equal to the R^2 value for the cut width.

IV. Discussion

The first test run was the scalloping test. From Fig. 3, it is clear that there is not any evidence of pronounced scalloping, which is often seen in cuts made at low PPI settings. This may have an important impact on the use of CO_2 laser-cut PDMS in lab-on-a-chip applications, due to its effect on flow characteristics.

The two outside radius profiles and the two slope profiles were obtained to gain a better understanding of the differences between the left and right sides of the cut profile. When using the MATLAB program to fit circles, sharp corners had radii that were less than 22 micrometers. The majority of values for radius 1 were less than 22; this means that the left side of the cut profile was often very steep, with a somewhat sharp corner at the intersection of the cut and the surface of the PDMS sheet, as seen in Fig. 6. Radius 3 was often much larger, with values going as high as 175 micrometers. This shows how smooth the transition from the top side to the cut was on the right hand side. This pattern of a sharp corner on the left side and a smooth arc on the right side was present on many of the cuts. This skew may have been due to a small, constant asymmetric Gaussian laser profile at the point of cutting. This assertion is supported by the data obtained for slope 1 and slope 2. Slope 1, on the left side of the cut profile, had a greater average magnitude than slope 2. This shows that the left side was usually steeper than the right side. This asymmetry was most likely not a function of the assist gas because air was supplied coaxially. One possible explanation for asymmetry in the cut profile is an inherent non-perpendicularity of the laser to the cutting surface.

Data for radius 2 was obtained in order to understand the properties of the bottom of the channel. This model was appropriate due to the fact that nearly all of the cuts had an arc-shaped profile at their bottom. The general trend for this bottom circle was as the power increased, the radius decreased. This is probably due to the fact that as the laser became more powerful, it cut deeper, which essentially 'buried' the bottom of the profile. An important exception is on profiles where the laser cut through the entire PDMS sheet. In these cases, the laser expanded the channel width once it had cut through the entire height, making the projected radius of the bottom of the channel much larger.

Data obtained for cut depth and width exposed some interesting trends in data. Figs. 10 and 11 show extremely strong linear relationships between cut depth and laser power. One important thing to note about cut depth was that for several of the high power/low speed cuts, the laser penetrated the entire thickness of the PDMS sheet. Once this happened, no attempt was made to extrapolate actual cut depth for fear of inaccuracy. Instead, cut depth is measured to be the height of the PDMS sheet. This trend is clear in Figs. 10 and 11 at the high end of the cut depth spectrum. Cut width charts showed a clear increase in cut width as laser power increased. These relationships also exhibited strong linear characteristics.

Both procedural and measurement error are suspected to

have been a factor in the results shown in the charts. Procedural error mainly involves the direction of the laser cut, while measurement error is a factor of the inherent human error involved in taking measurements. In order to reduce procedural error, an experiment has been proposed in which ablation profile is determined as a function of radial direction. In order to reduce measurement error, further MATLAB programming will include functions which automatically detect edges and make depth and width measurements.

One important observation made was the amount of bulging found around the edges of the cuts. In past experiments, bulging in CO_2-cut polymers has been a cause for concern, as irregularities around the edges of the cuts have induced flow problems in channels, as well as introduced difficulties in the bonding process. Chung, Lin, and Huang expounded on the bulge effect in PMMA, and proposed a PDMS coating to reduce it [9]. In this research, no bulge formation was noted, which makes this type of PDMS channel ideal for lab-on-a-chip applications. Furthermore, because of the elastic nature of PDMS, any small bulge formations could be reduced during bonding with simple mechanical pressure.

V. Conclusion

The conclusions drawn in this research have important implications in microfluidics. We have demonstrated that carbon dioxide laser-cut PDMS has the characteristics that make it a viable substrate for lab-on-a-chip applications due to its rounded channel profile and smooth edges. We assert that this will enable patterning of microfluidic networks at low cost and high automation throughput. While femtosecond lasers define the limit of fabrication resolution in laser microfabrication, it is imperative when transitioning to automated systems that cost be optimized. We have demonstrated that for a class of manufacturing configurations relevant to lab-on-a-chip integrated systems that carbon dioxide lasers are cost effective and excellent for this process. Further research will focus on flow characteristics within these PDMS channels, something that has not yet been analyzed. As well, further study of trends within the cut profile pertaining to the three radii is planned. Another possible direction for future research is the potential for the establishment of linear regressions for the modeling of channel width and depth based on the changeable parameters of the laser. This will allow future researchers to be able to look up the optimum laser settings for cutting once they have chosen a channel depth. Further future research will also include techniques for determining the characteristics of the entire channel, using a combination of SEM and optical surface profilometry. This research will further aid lab-on-a-chip applications by giving insights into overall channel characteristics, surface porosity, and residue in and around the channel. Further research will also look to understand the effect of laser machining on the surface chemistry of PDMS. Because water-based microfluidics often calls for hydrophilic channels, the ability to fabricate them is extremely important.

Acknowledgment

We would like to acknowledge the editing assistance provided by Dr. Roger Johnson and the support of The Biodesign Institute staff, with special recognition to Steve Fay.

References

[1] C. G. Khan Malek, "Laser processing for bio-microfluidics applications (part II)," *Anal Bioanal Chem*, vol. 385 , pp. 1362-1369, June 2006.

[2] D.B. Wolfe, J.B. Ashcom, J.C. Hwang, C.B. Schaffer, E. Mazur, G.M. Whitesides, "Customization of poly(dimethylsiloxane) stamps by micromachining using a femtosecond-pulsed laser," *Advanced Materials*, vol. 5, pp. 62-65, January 2003.

[3] T.N. Kim, K. Campbell, A. Groisman, D. Kleinfeld, C.B.Schaffer, "Femtosecond laser-drilled capillary integrated into a microfluidic device," *Applied Physics Letters*, vol. 86, pp. 1-3, May 2005.

[4] M.N. Nguyen, H.D. Fahlenkamp, R.G. Higbee, A.M. Kachurin, K.H. Church, W.L. Warren, "Laser machined microfluidic bioreactors with printed scaffolds and integrated optical waveguides," *Proceedings of SPIE*, vol. 5591, pp. 104-112, 2004.

[5] S.H. Chan, N.T. Nguyen, Z. Xia, Z. Wu, "Development of a polymeric micro fuel cell containing laser-micromachined flow channels," *Journal of Micromechanics and Microengineering*, vol. 15, pp. 231-236, October 2004.

[6] D.L. Pugmire, E.A. Waddell, R.Haasch, M.J. Tarlov, L.E. Locascio, "Surface characteraization of laser-ablated polymers used for microfluidics," *Anal. Chem*, vol. 74, pp. 871-878, January 2002.

[7] D. Pham, L. Tonge, J. Cao, J. Wright, M. Papiernik, E. Harvey, D. Nicolau, "Effects of polymer properties on laser ablation behaviour," *Smart Mater. Struct.*, vol. 11, pp. 668-674, July 2002.

[8] V.M. Graubner, R. Jordan, O. Nuyken, T. Lippert, M. Hauer, B. Schnyder, A. Wokaun, "Incubation and ablation behavior of poly(dimethylsiloxane) for 266 nm irradiation," *Applied Surface Science*, vol. 197-198, pp. 786-790, 2002.

[9] C.K. Chung, Y.C. Lin, G.R. Huang, "Bulge formation and improvement of the polymer in CO_2 laser micromachining," *J. Micromech. Microeng.*, vol. 15, pp. 1878-1884, August 2005.

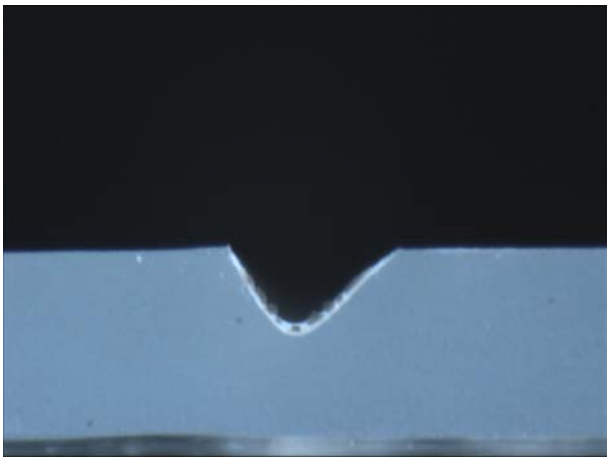

Fig. 1. Channel cross-section (60% power setting, 50% speed setting, 750 PPI).

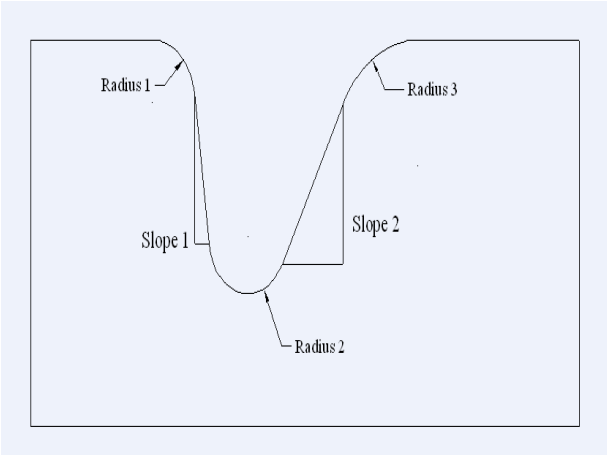

Fig. 2. Cross section topography descriptors. Radius 1 and radius 3 illustrate the nature of the transition from PDMS surface to cut, while radius 2 illustrates the nature of the bottom of the channel.

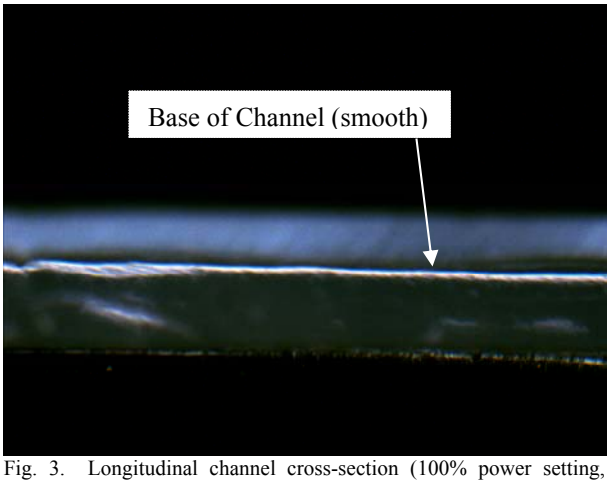

Fig. 3. Longitudinal channel cross-section (100% power setting, 100% speed setting, 500 PPI), showing an absence of scalloping.

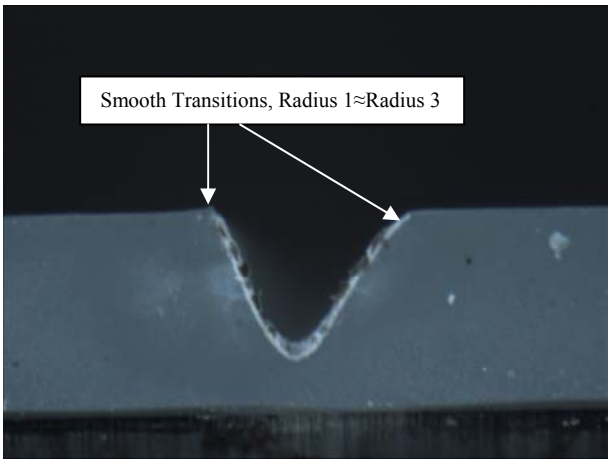

Fig. 4. Channel cross-section (90% power setting, 50% speed setting, 750 PPI), showing approximate Gaussian profile.

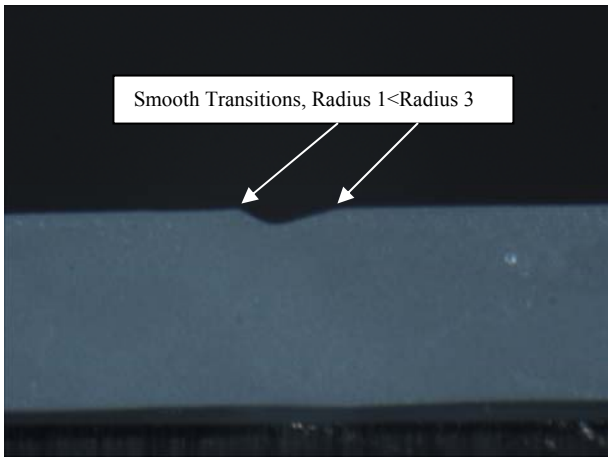

Fig. 5. Channel cross-section (20% power setting, 50% speed setting, 500 PPI), showing configuration with radius 3 greater than radius 1.

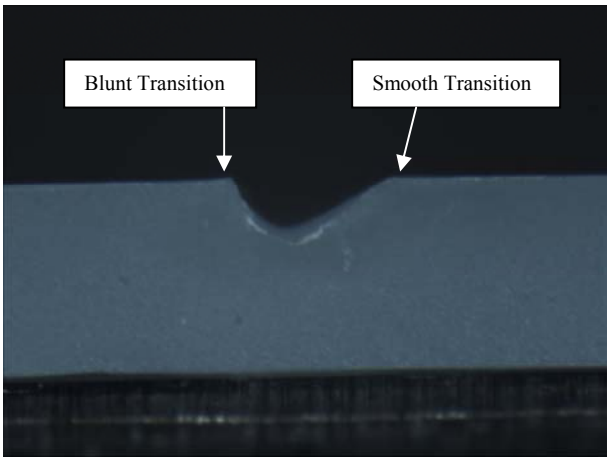

Fig. 6. Channel cross-sectional (70% power setting, 100% speed setting, 500 PPI), showing slope 1 greater than slope 2.

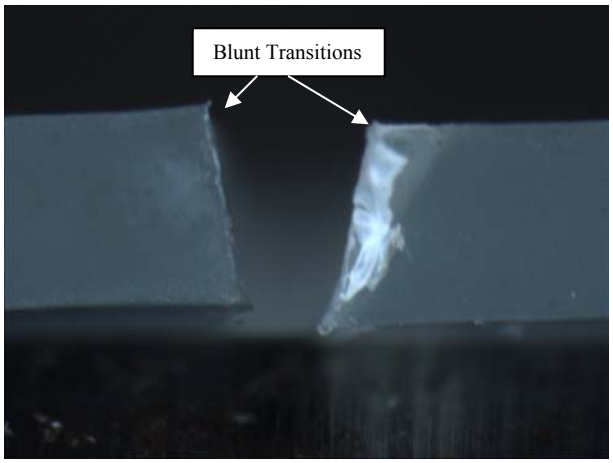

Fig. 7. Channel cross-section (100% power setting, 25% speed setting, 750 PPI). Full-thickness cut due to high power deposition.

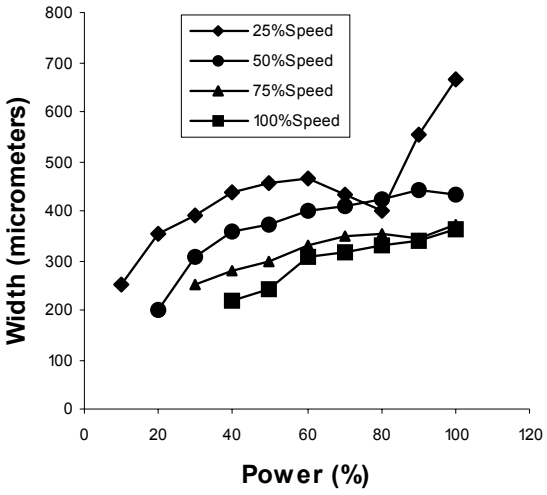

Fig. 8. Width vs. laser power setting for various speed settings at 500 PPI.

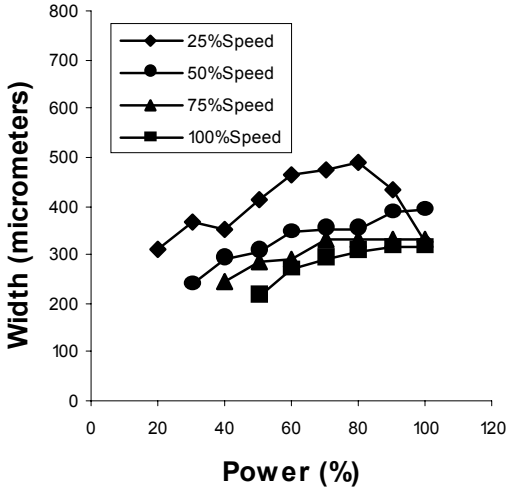

Fig. 9. Width vs. laser power setting for various speed settings at 750 PPI.

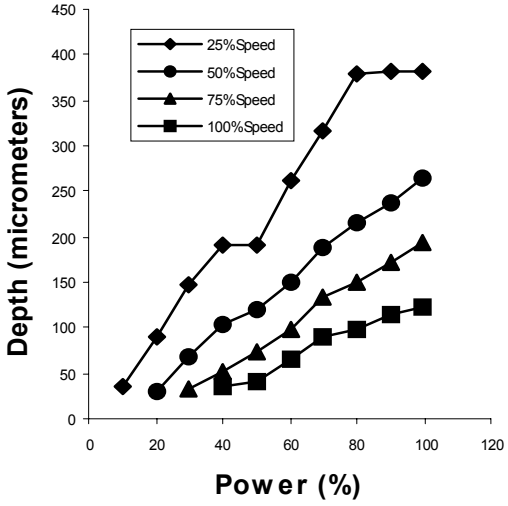

Fig. 10. Depth vs. laser power setting for various speed settings at 500 PPI.

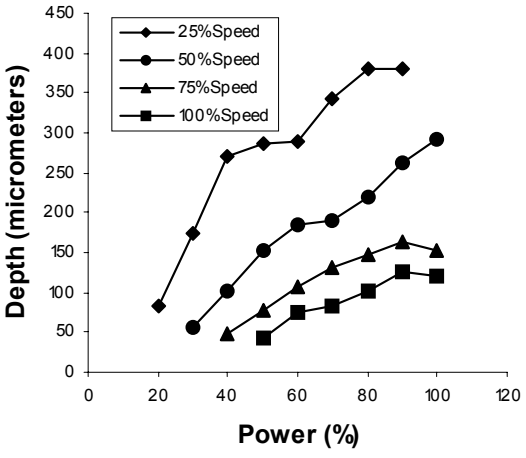

Fig. 11. Depth vs. laser power setting for various speed settings at 750 PPI.

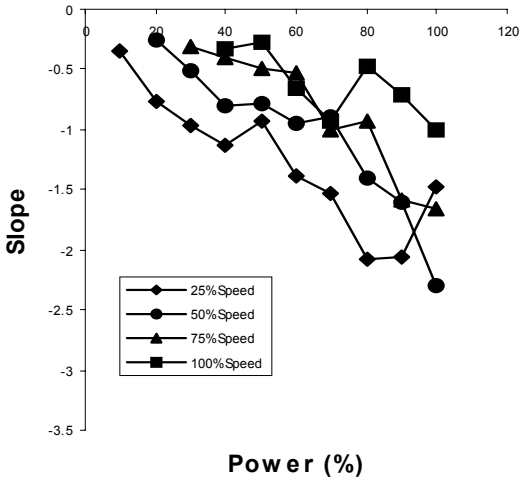

Fig. 12. Slope 1 vs. laser power setting for various speed settings at 500 PPI.

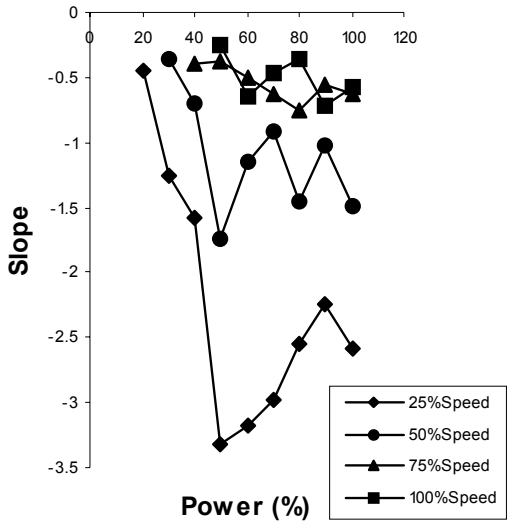

Fig. 13. Slope 1 vs. laser power setting for various speed settings at 750 PPI.

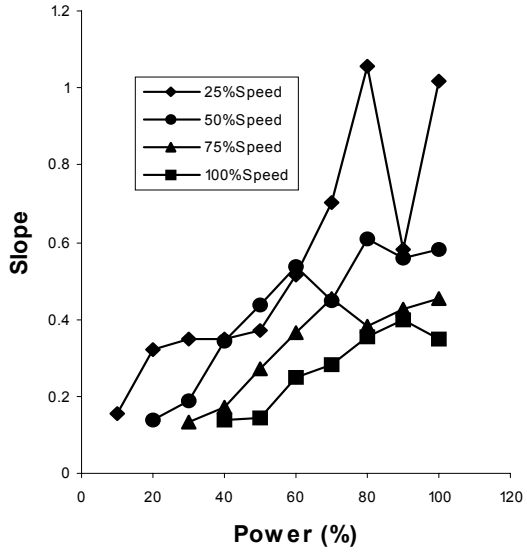

Fig. 14. Slope 2 vs. laser power setting for various speed settings at 500 PPI.

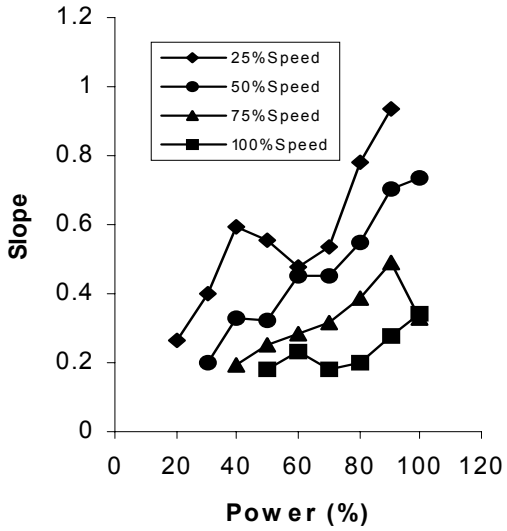

Fig. 15. Slope 2 vs. laser power setting for various speed settings at 750 PPI.